Modeling and Simulation Analysis of Dual-Rotor Vibration System with Multiple Faults

Yizhou Yang, Chao Liu, Dongxiang Jiang and Wenguang Yang
State Key Lab of Control and Simulation of Power Systems and Generation Equipment,
Department of Thermal Engineering, Tsinghua University
Beijing 100084, China
Telephone: +86 15201522492
yangyz16@mails.tsinghua.edu.cn

Abstract: Dual-rotor system is an important rotor form in rotating machinery like gas turbine engine. Its complex structure results in rich dynamical behaviors and more probability to failure. The modeling and simulation of the dual-rotor system can help to understand its dynamic characteristics and provide theoretical support for the design, operation and maintenance. In this paper, a dynamic model of a dual-rotor system with multiple rotor faults is established. The dual-rotor vibration model without any fault is built by finite element method, where the two shafts are connected by an inter-shaft bearing and nonlinear models of rolling element bearing and squeeze film damper are considered. The numerical integration method of Newmark-β is used to obtain the steady-state vibration response of the system. Then rotor faults are introduced to the system model, including unbalance, misalignment, looseness and rub-impact. The steady-state responses of single faults in the dual-rotor system are analyzed and typical fault features are obtained. Then coupling characteristics between different rotor faults, and the influences of the squeeze film dampers on the dynamic characteristics and fault features of the system are studied.

Keywords: dual-rotor system, modeling and simulation, rotor faults, rolling element bearing, squeeze film damper.

Introduction: Dual-rotor is a common form of rotor system in rotating machinery like aero-engines. The high-pressure rotor and the low-pressure rotor are coupled via an inter-shaft bearing, and the speed of the rotors are different and variable, making the vibration signals more complex than general rotating machinery. The modeling and simulation of the dual-rotor system and rotor faults can help to understand their dynamic characteristics and provide theoretical support for the design, operation and maintenance of the rotor. The finite element model turn the continuous flexible structure into finite discrete elements, obtains rich internal information, and are also convenient to add nonlinear forces, which is suitable for numerical calculation [1, 2]. Processing the flexible parts as finite elements and the parts of large stiffness as discrete lumped masses could reduce the complexity of the

system model and ensure the accuracy of simulation results at the same time, making it a more efficient modeling approach [3, 4].

Rolling element bearings and squeeze film dampers are introduced in rotor models in forms of nonlinear external forces. The earliest complete rolling element bearing model was established by Gupta in 1975, which had 2 degrees of freedoms (DOFs) and Hertzian contact, the non-linearity and time-varying characteristics are considered in. Later more nonlinear factors had been taken into consideration in this bearing force model by other researchers, like bearing race clearance and the rolling element slippage. Squeeze film damper is a type of fluid-film bearing whose simplest form consists of an oil-filled annular cavity surrounding the outer race of a rolling element bearing. In aero-engines where rolling element bearings provide little damping, squeeze film dampers are widely used to introduce additional damping to attenuate vibration. The cavitated short bearing theory is employed for calculating the fluid-film forces in a damper, as the outer race of the bearing acts as the damper's journal and is prevented from rotating but allowed to whirl.

In this paper, a finite element approximate model of an aero-engine dual-rotor system which includes nonlinear models of rolling element bearings and squeeze film dampers are established. Steady-state vibration response of the dual-rotor system is obtained by solving the dynamic equation of the system. Then models of typical rotor faults are introduced to the system by adding nonlinear forces to the generalized external force vector. Simulated faults include rotor unbalance, rotor misalignment, support looseness, and dynamic-static rub-impact. Vibration responses of single rotor faults are calculated and fault features are obtained. Those fault features are compared with situations with the absence of squeeze film dampers. Vibration responses of situations with more than one rotor fault are calculated, whose fault features are also compared with ones of single fault situations.

Dynamic model of the dual-rotor system: The dual-rotor system consists of two rotors connected by an inter-shaft bearing. Each rotor is composed of a flexible shaft, rigid discs and supports. The schematic of the rotor system is shown in Figure 1. The support arrangement of the rotor is similar to the actual aero-engine rotor.

The shafts are modelled with finite element method by using the 3-D elastic beam element. The 3-D elastic beam element has 2 nodes and each node has 6 degree of freedoms (DOFs), which are translations in the X, Y and Z directions and rotations around the X, Y and Z directions. The DOFs and the motion equation of the element are:

$$q^{\mathrm{e}} = \left[u_{x1}, u_{y1}, u_{z1}, \theta_{x1}, \theta_{y1}, \theta_{z1}, u_{x2}, u_{y2}, u_{z2}, \theta_{x2}, \theta_{y2}, \theta_{z2}\right]^T \quad (1)$$

$$M^e\ddot{q}^e + (-\omega G^e)\dot{q}^e + K^e q^e = 0 \quad (2)$$

M^e is the consistent mass matrix, G^e is the gyroscopic matrix, K^e is the stiffness matrix and ω is the rotational speed.

The rigid discs are modelled as discrete lumped masses using the 3-D mass element which has one node with 6 DOFs. The DOFs and the motion equation of the element are:

$$q^{\mathrm{e}} = \left[u_x, u_y, u_z, \theta_x, \theta_y, \theta_z\right]^T \tag{3}$$

$$M^e \ddot{q}^e + (-\omega G^e)\dot{q}^e = Q^e \tag{4}$$

Q^e is the external force vector and could be the unbalance force or other types of excitation on the disc.

As shown in the Figure 1, the shaft of the low-pressure (inner) rotor has been divided into 17 elements and has 18 nodes, and the shaft of the high-pressure (outer) rotor has been divided into 18 elements and has 19 nodes. The shafts lie along the X direction. Combine all the elements of a shaft and discs together, the motion equation of one rotor is:

$$M_i^r \ddot{q}_i^r + (C_i^r - \omega_i G_i^r)\dot{q}_i^r + K_i^r q_i^r = Q_i^r, \qquad i = 1{,}2 \tag{5}$$

C^r is the damping matrix which is using Rayleigh damping for simplicity and is in the form of proportional damping [5] as:

$$C^r = \alpha M^r + \beta K^r \tag{6}$$

The rotor system model is established by assembling all the finite elements and add the external forces. The motion equation could be written as:

$$M^s \ddot{q}^s + (C^s - \omega G^s)\dot{q}^s + K^s q^s = Q^s \tag{7}$$

Q^s is the generalized external force vector of the system, which contains the unbalance forces, the weight forces, and the nonlinear forces of the rolling element bearings and the squeeze film dampers:

$$Q^s = F_u + W - F_B + F_D \tag{8}$$

The unbalance force on the disc is the main excitation of this dynamic model. The nonlinear equation of the rotor system model is solved by the explicit Newmark-β method. This numerical integration approach is suitable for obtaining the dynamic response of a nonlinear system. Then the displacement, velocity and acceleration at each node of the finite element model can be obtained.

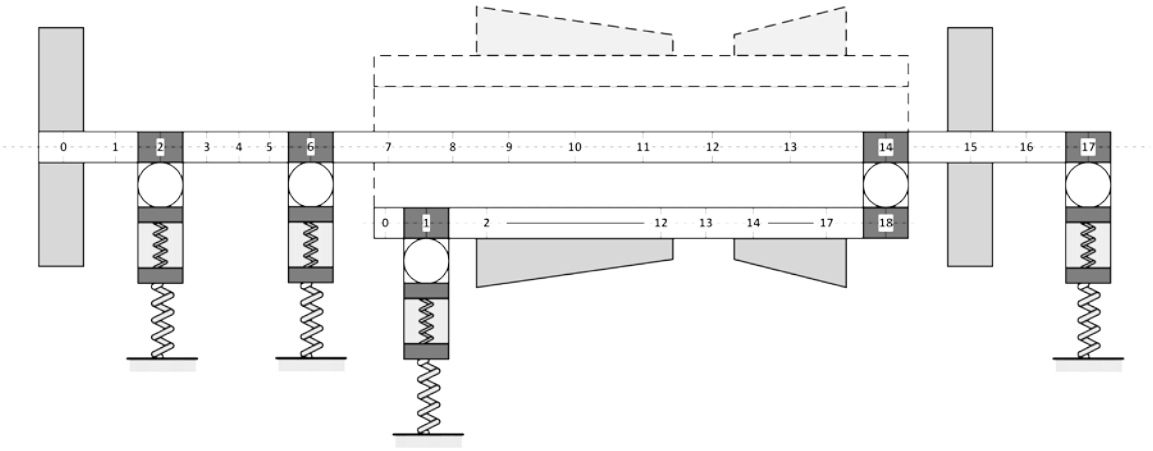

Figure 1. Dual-rotor system model.

Rolling element bearing model: The rotor is supported by rolling element bearings. Here a nonlinear multi-body dynamic model is used [6, 7], which is shown in Figure 2. The

rolling element bearing model is assumed as nonlinear springs with no mass and evenly arranged along the rolling element raceway. The inner race of the bearing is assumed to be fixed to the shaft and the outer race is modelled as a lumped mass.

When the rotor rotates at constant speed of ω, the cage speed is ω_c. The angular position of the ith rolling element at time t will be θ_i.

$$\omega_c = \frac{\omega}{2}\left(1 - \frac{d}{D}\cos\alpha\right) \tag{9}$$

$$\theta_i = \frac{2\pi(i-1)}{Z} + \omega_c t + \theta_0 + (0.5 - rand) \times \theta_{slip} \quad i = 1, 2, \dots Z \tag{10}$$

θ_0 is the initial position of the first rolling element. $(0.5 - rand) \times \theta_{slip}$ is the phase deviation caused by slippage. The value of phase variation θ_{slip} could be 0.01 ~ 0.02 rad. If the displacement of the shaft (x_s, y_s) and the outer race (x_o, y_o) is known, the contact deformation for the ith rolling element is given as:

$$\gamma_i = (x_s - x_o)\cos\theta_i + (y_s - y_o)\sin\theta_i - \delta \quad i = 1, 2, \dots Z \tag{11}$$

δ is the initial clearance between the rolling elements and the bearing races. The rolling elements are compressed only when γ_i is positive, so the contact deformation will be multiplied by a factor as:

$$\lambda_i = \begin{cases} 1 & \gamma_i > 0 \\ 0 & \gamma_i \le 0 \end{cases} \tag{12}$$

According to Hertzian contact theory, the contact force of the ith rolling element is:

$$f_i = k_b(\lambda_i\gamma_i)^n \tag{13}$$

k_b is the contact stiffness factor and can be obtained from geometric and material properties of the contact between the rolling element and the inner race or the outer race. The exponent n is 3/2 when the bearing is a ball bearing and 10/9 when a roller bearing. The total bearing force can be calculated by summing the contact force of each rolling element in the X and Y directions:

$$\begin{cases} F_{Bx} = k_b \sum_{i=1}^{Z} (\lambda_i\gamma_i)^n \cos\theta_i \\ F_{By} = k_b \sum_{i=1}^{Z} (\lambda_i\gamma_i)^n \sin\theta_i \end{cases} \tag{14}$$

Squeeze film damper model: The squeeze film damper (SFD) is mounted between the outer race of a rolling element bearing and a bearing pedestal. The outer race forms the non-rotating journal of the squeeze film damper, and are supported by centering strings [8-10]. The model of SFD is shown in Figure 2.

Theoretical oil-film forces in squeeze film dampers are obtained by integrating the pressure distribution over the entire damper surface. Based on the Reynolds equation and the short bearing approximation, the pressure distribution in a π-film damper may be derived as:

$$p(\theta,z)=-\frac{6\mu}{c^2}\left(\frac{L^2}{4}-z^2\right)\frac{\varepsilon\dot{\phi}\sin\theta+\dot{\varepsilon}\cos\theta}{(1+\varepsilon\cos\theta)^3} \tag{15}$$

In the equation, ε and $\dot{\varepsilon}$ respectively are the eccentricity ratio and velocity in the radial direction. $\dot{\phi}$ is the angular velocity. θ is the angular position measured from the maximum film thickness end of the line of centers. L is the length of the damper, z the position in the axial direction, c the damper's radial clearance, and μ the dynamic viscosity of the oil.

Positive pressures occur for $\theta_1<\theta<\theta_1+\pi$ when

$$\varepsilon\dot{\phi}\sin\theta+\dot{\varepsilon}\cos\theta<0 \;\; and \;\; \tan\theta_1=\frac{\dot{\varepsilon}}{-\varepsilon\dot{\phi}} \tag{16}$$

Then the oil film forces can be integrated as:

$$F_r=-\frac{\mu R L^3}{c^2}\left(\dot{\varepsilon}I_1+\varepsilon\dot{\phi}I_2\right) \tag{17}$$

$$F_t=-\frac{\mu R L^3}{c^2}\left(\dot{\varepsilon}I_2+\varepsilon\dot{\phi}I_3\right) \tag{18}$$

where

$$I_1=\int_{\theta_1}^{\theta_1+\pi}\frac{\cos^2\theta}{(1+\varepsilon\cos\theta)^3}d\theta \tag{19}$$

$$I_2=\int_{\theta_1}^{\theta_1+\pi}\frac{\cos\theta\sin\theta}{(1+\varepsilon\cos\theta)^3}d\theta \tag{20}$$

$$I_3=\int_{\theta_1}^{\theta_1+\pi}\frac{\sin^2\theta}{(1+\varepsilon\cos\theta)^3}d\theta \tag{21}$$

The closed form expressions of the integrals have been evaluated analytically as:

$$I_1=\frac{\varepsilon\sin\theta_1\,(3+(2-5\varepsilon^2)\cos^2\theta_1)}{(1-\varepsilon^2)^2(1-\varepsilon^2\cos^2\theta_1)^2}+\frac{\alpha(1+2\varepsilon^2)}{(1-\varepsilon^2)^{2.5}} \tag{22}$$

$$I_2=-\frac{2\varepsilon\cos^3\theta_1}{(1-\varepsilon^2\cos^2\theta_1)^2} \tag{23}$$

$$I_3=\frac{\varepsilon\sin\theta_1\,(1+(\varepsilon^2-2)\cos^2\theta_1)}{(1-\varepsilon^2)(1-\varepsilon^2\cos^2\theta_1)^2}+\frac{\alpha}{(1-\varepsilon^2)^{1.5}} \tag{24}$$

$$\alpha=\frac{\pi}{2}+\arctan\left[\frac{\varepsilon\sin\theta_1}{(1-\varepsilon^2)^{0.5}}\right] \tag{25}$$

Suppose the displacement of the outer race (x_o,y_o) and the bearing pedestal (x_p,y_p), and the velocity of the outer race $(\dot{x}_o,\dot{y}_o)$ and the bearing pedestal $(\dot{x}_p,\dot{y}_p)$, so

$$x=x_o-x_p,\qquad y=y_o-y_p \tag{26}$$

$$\dot{x}=\dot{x}_o-\dot{x}_p,\qquad \dot{y}=\dot{y}_o-\dot{y}_p \tag{27}$$

$$\varepsilon = \frac{e}{c} = \frac{\sqrt{x^2 + y^2}}{c}, \qquad \dot{\varepsilon} = \frac{x \cdot \dot{x} + y \cdot \dot{y}}{c\sqrt{x^2 + y^2}} \tag{28}$$

$$\phi = \arctan\frac{y}{x}, \qquad \dot{\phi} = \frac{x \cdot \dot{y} - y \cdot \dot{x}}{\sqrt{x^2 + y^2}} \tag{29}$$

The oil-film forces in polar coordinates can be recast in Cartesian coordinates like:

$$\begin{cases} F_{Dx} = F_r \cos\phi - F_t \sin\phi \\ F_{Dy} = F_r \sin\phi + F_t \cos\phi \end{cases} \tag{30}$$

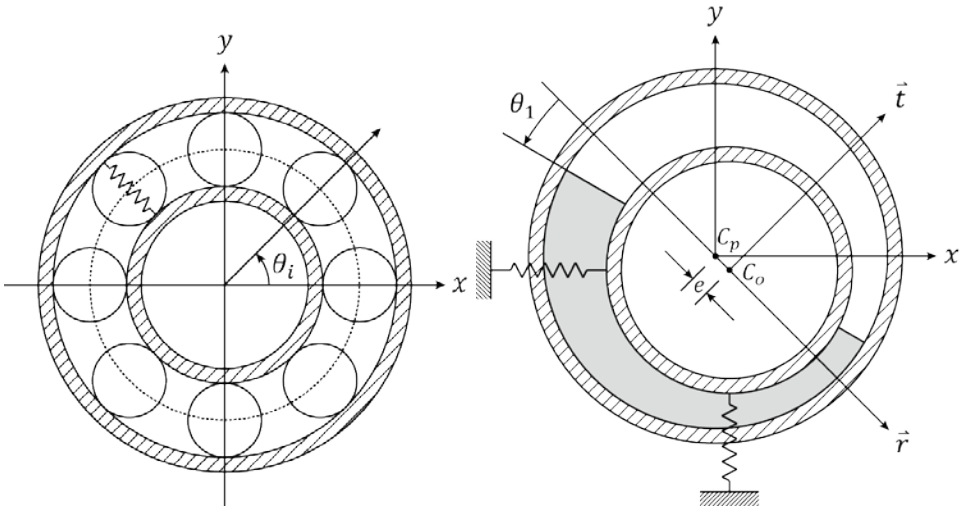

Figure 2. Rolling element bearing and squeeze film damper model.

Table 1. Parameters of rolling element bearing and squeeze film damper model.

Model	Notation	Description	Value	
Rolling element bearing	D	Pitch diameter	306 mm	
	d	Rolling element diameter	17 mm	
	Z	Rolling element number	30	
	α	Contact angle	0	
	k_b	Contact stiffness factor	7×10^8 N·m$^{-3/2}$	6×10^7 N·m$^{-10/9}$
Squeeze film damper	μ	Dynamic viscosity of oil	5 mPa·s	
	R	Damper radius	180 mm	
	L	Damper length	42 mm	
	c	Damper radial clearance	0.36 mm	

Normal state vibration response: Vibration response of the dual-rotor system without any rotor fault is calculated. The rotating speed is set to a fixed value of (70, 90) Hz. The displacement waveform, spectrum and shaft centerline orbit of node 0 and node 15 on the inner rotor are in Figure 3. Due to the coupling effect of the inter-shaft bearing, both

frequencies of the rotating speed are reflected on the same node. Node 15 is near the inter-shaft bearing than node 0, so the spectral line of the outer shaft frequency is higher than the one of the inner shaft frequency, and vice versa. Besides the two main frequencies, no other frequency components is clear in the vibration signals.

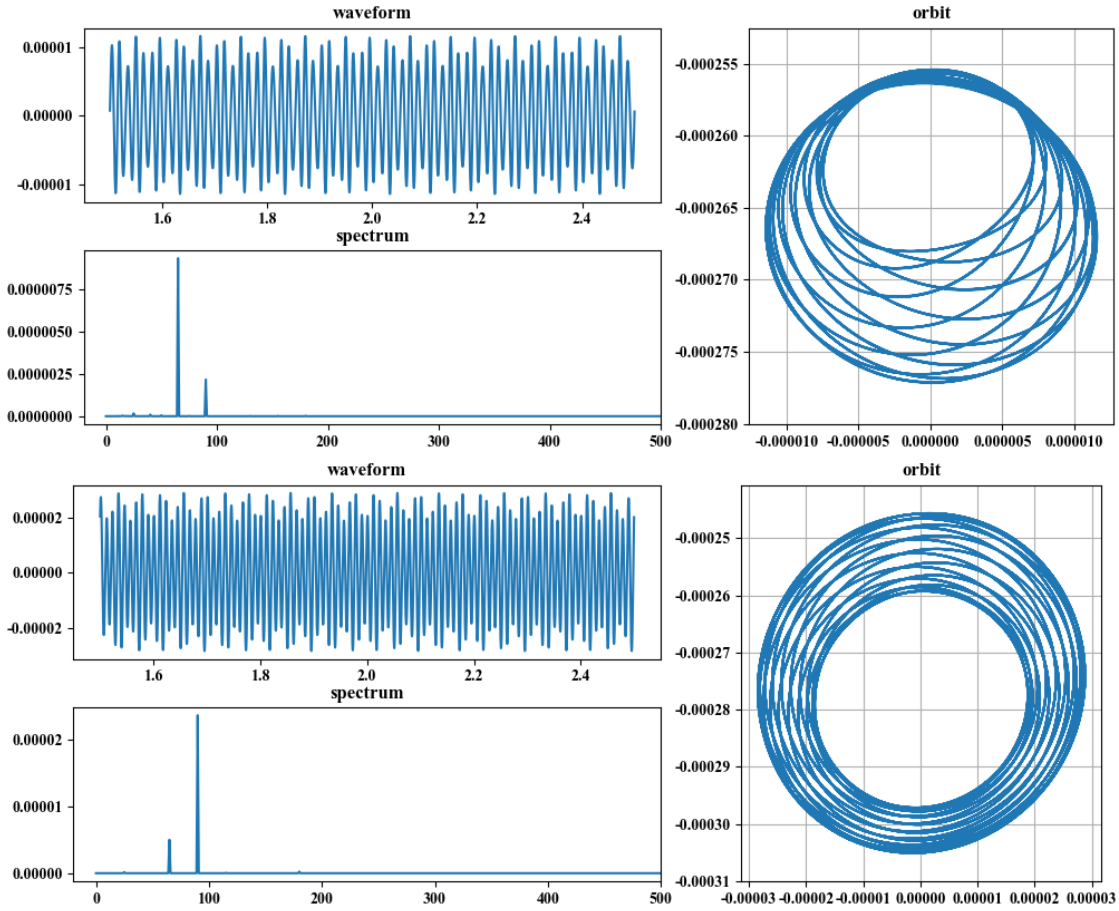

Figure 3. Waveform, spectrum and orbit of node 0 and node 15 on the inner rotor.

Some states are considered including: (1) no gravity effect, (2) no squeeze film damper, (3) SFD has no centering string, (4) centering string has have the stiffness. Vibration responses of those states are calculated and their shaft centerline orbits of the outer race (journal of SFD) of support 3 and node 3 at the outer rotor are plotted in Figure 4, comparing with the normal state. If the gravity effect is neglected, the shaft centerline orbit will be centered on the origin. When there is gravity or the stiffness of the SFD centering string is weakened, the center of orbit declines. And if there are no SFD in the dual-rotor system, the trajectory of the rotor will be relatively messy, and the inner rotor frequency become more prominent because there are three SFDs on the inner rotor but only one on the outer rotor. It can be seen that the damping effect of the squeeze film damper is very significant.

Calculate vibration responses at different rotating speed with a speed ratio of 1.5. All the spectra are plotted in the 3D spectrum of Figure 5. As the rotating speed increases, the

vibration amplitude will increase significantly as the two rotational frequencies pass through the natural frequencies of the dual-rotor system. When the rotating speed is about (20, 30) and (56, 84) Hz the outer rotor has a high vibration amplitude. When the rotating speed is about (32, 48) and (84, 126) Hz the inner rotor has a high vibration amplitude. Thus it can be inferred that the first two natural frequencies is around 31 and 84 Hz.

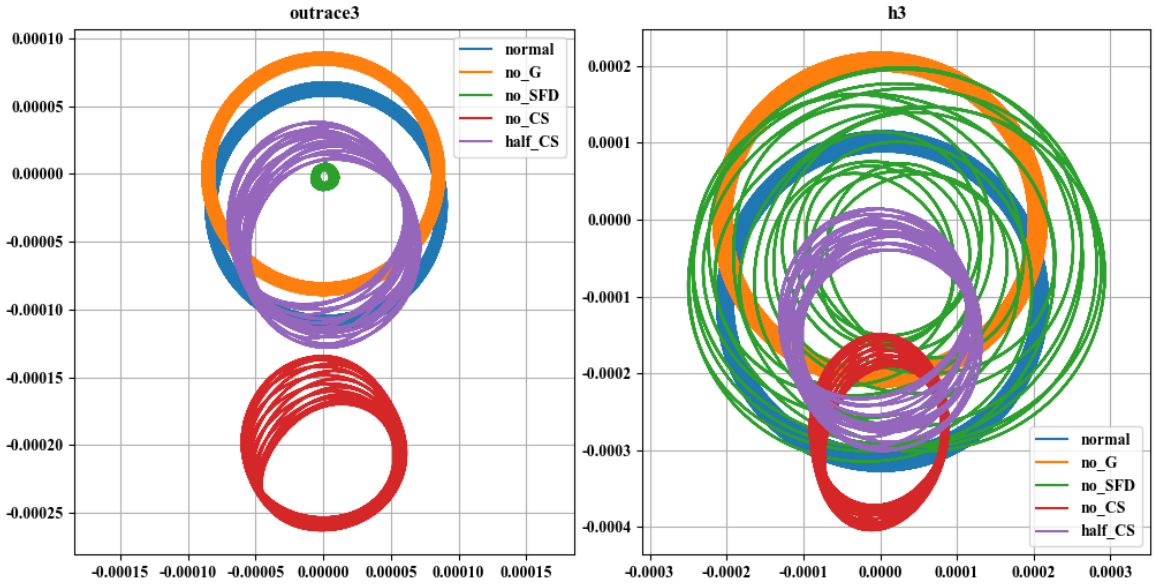

Figure 4. Shaft centerline orbits of the outer race 3 and node 3 at the outer rotor.

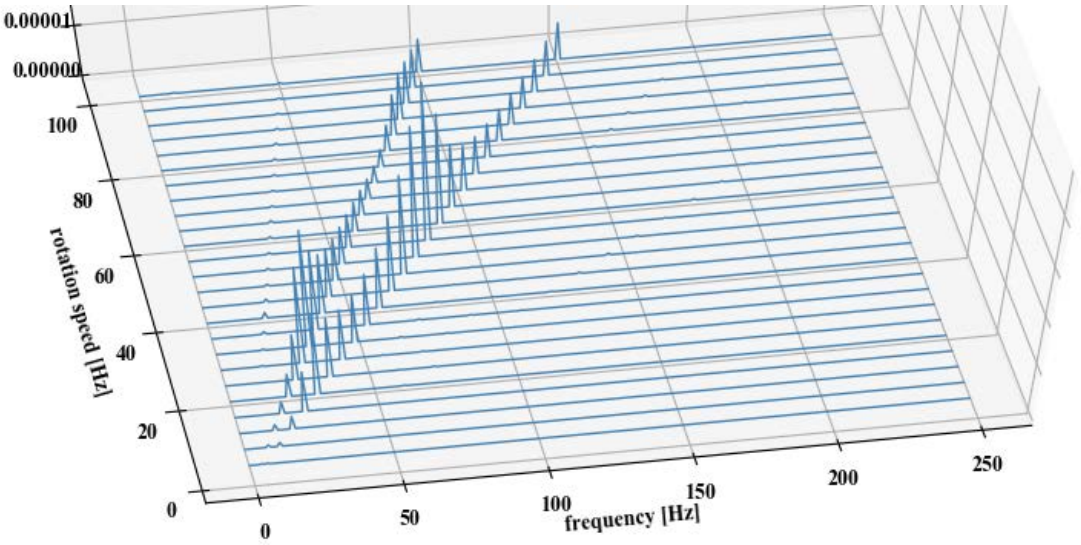

Figure 5. 3D spectrum at different rotating speed with a speed ratio of 1.5.

Models of rotor faults: Typical rotor faults include rotor unbalance, rotor misalignment, support looseness, and dynamic-static rub-impact. In the dual-rotor system dynamics model, a typical rotor fault is achieved by adding a corresponding load in the generalized external force vector.

Rotor unbalance manifests as centrifugal forces of the eccentric mass. Unbalance force is often the main excitation of a rotor dynamic system, but large eccentric mass will cause excessive vibration when the rotor rotates at a high speed. The external force of the unbalance fault model is:

$$\begin{cases} F_{uiy} = m_{di} e\omega^2 \cos(\omega t) \\ F_{uiz} = m_{di} e\omega^2 \sin(\omega t) \end{cases} \tag{31}$$

Rotor misalignment happens when two rotors connected by a coupling do not have their axes on the same line. The coupling will rotate as an eccentric mass at twice the rotor speed, adding a misalignment force to the rotor [11]. The external force of the misalignment fault model is:

$$\begin{cases} F_{miy} = -m_{ci} e\omega^2 \sin(2\omega t) \\ F_{miz} = m_{ci} e\omega^2 \cos(2\omega t) \end{cases} \tag{32}$$

Support looseness leads to a reduction in the stiffness of the connection and even creates an unconstrained gap. So the looseness fault manifests as piecewise linear stiffness of the foundation support [12]. The external force of the looseness fault model is:

$$F_{li} = \begin{cases} (k_0 - k_{l1}) \cdot x_i & x_i > d_l \\ (k_0 - k_{l2}) \cdot x_i & x_i \le 0 \\ k_0 \cdot x_i & 0 < x_i \le d_l \end{cases} \tag{33}$$

Dynamic-static rub-impact is the friction and collision between the rotor and the stator due to the reduction of the clearance between them. When a rub-impact occurs, the moving part will come into contact with the static part and then spring back. The part with a lower material hardness will suffer greater wear as the rubbing progresses [13]. The external force of the rub-impact fault model is:

$$\begin{cases} F_{riy} = k_r(1 - d_r/r_i)(-y_i + f \cdot z_i) \\ F_{riz} = k_r\left(1 - d_r/r_i\right)(-z_i - f \cdot y_i) \end{cases} \quad r_i = \sqrt{y_i^2 + z_i^2} \ge d_r \tag{34}$$

Table 2. Parameters of rotor faults.

Fault	Parameter	Description	Value
Normal	e	eccentricity	0.02 mm / 0.01 mm
Unbalance	e	eccentricity	0.02 mm / 0.03 mm
Misalignment	$m_c e$	eccentric mass	0.004 mm·kg
Looseness	d_l	loose clearance	0.05 mm
	k_{l1}, k_{l2}	looseness stiffness	5×10^8 N/m
	k_0	clearance stiffness	0
Rub-impact	d_r	rotor-stator clearance	0.15 mm
	k_r	contact stiffness	7.5×10^7 N/m
	f	friction factor	0.1

Fault simulation results: Adding a single typical rotor fault in the dual-rotor system, the vibration response of each fault above is calculated. Parameters of the rotor faults used in the calculation are listed in Table 2.

The displacement waveform, spectrum and shaft centerline orbit of node 15 on the inner rotor at the state of unbalance fault is in Figure 6. The eccentric mass of the inner rotor disc increase, thus the amplitude of its rotation frequency increase. No other frequency component is added to the vibration signal. The shaft centerline orbit still looks smooth.

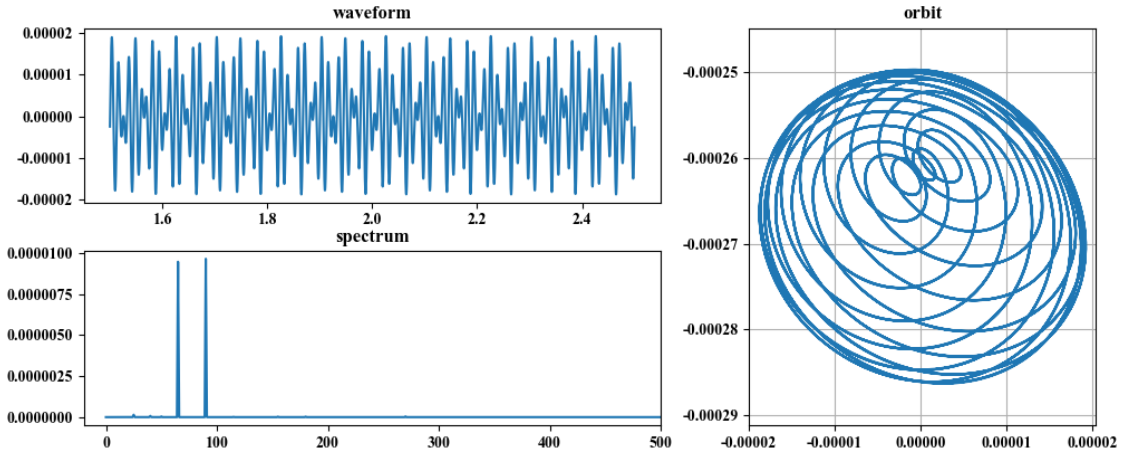

Figure 6. Waveform, spectrum and orbit of unbalance fault.

The displacement waveform, spectrum and shaft centerline orbit of node 15 on the inner rotor at the state of misalignment fault is in Figure 7. Due to the excitation of misalignment on the inner rotor, the frequency component of double the inner rotor rotation frequency becomes prominent.

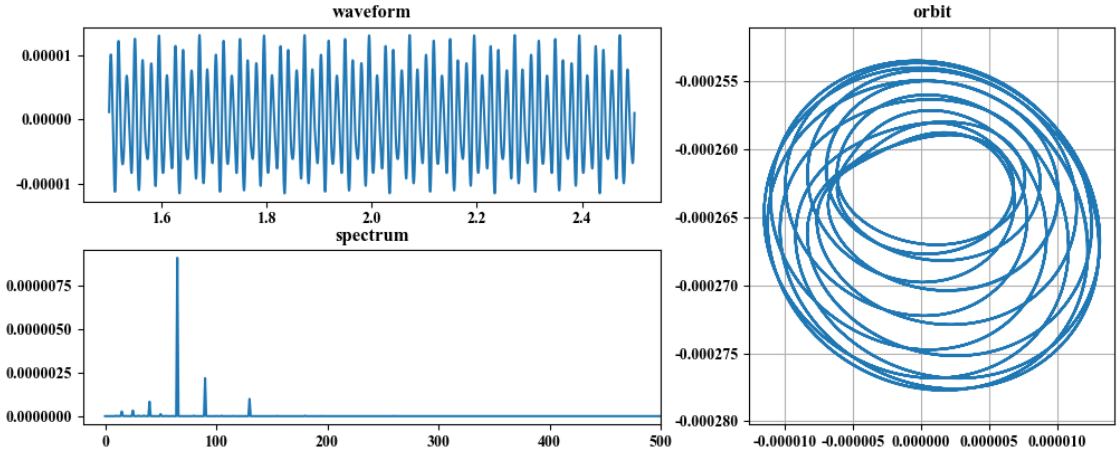

Figure 7. Waveform, spectrum and orbit of misalignment fault.

The displacement waveform, spectrum and shaft centerline orbit of node 15 on the inner rotor at the state of looseness fault is in Figure 8. The loose clearance is set in the horizon

direction, so the constraint in this direction weakens. Low frequency components below the rotation frequency appear in the spectrum.

When there is no squeeze film damper, fractional frequency components under the rotation frequency become more abundant. The shaft centerline orbit becomes less smooth. Looseness will cause a certain degree of impact vibration, but the presence of SFDs weakens the impact. This is also an important manifestation of the shock absorption of SFDs.

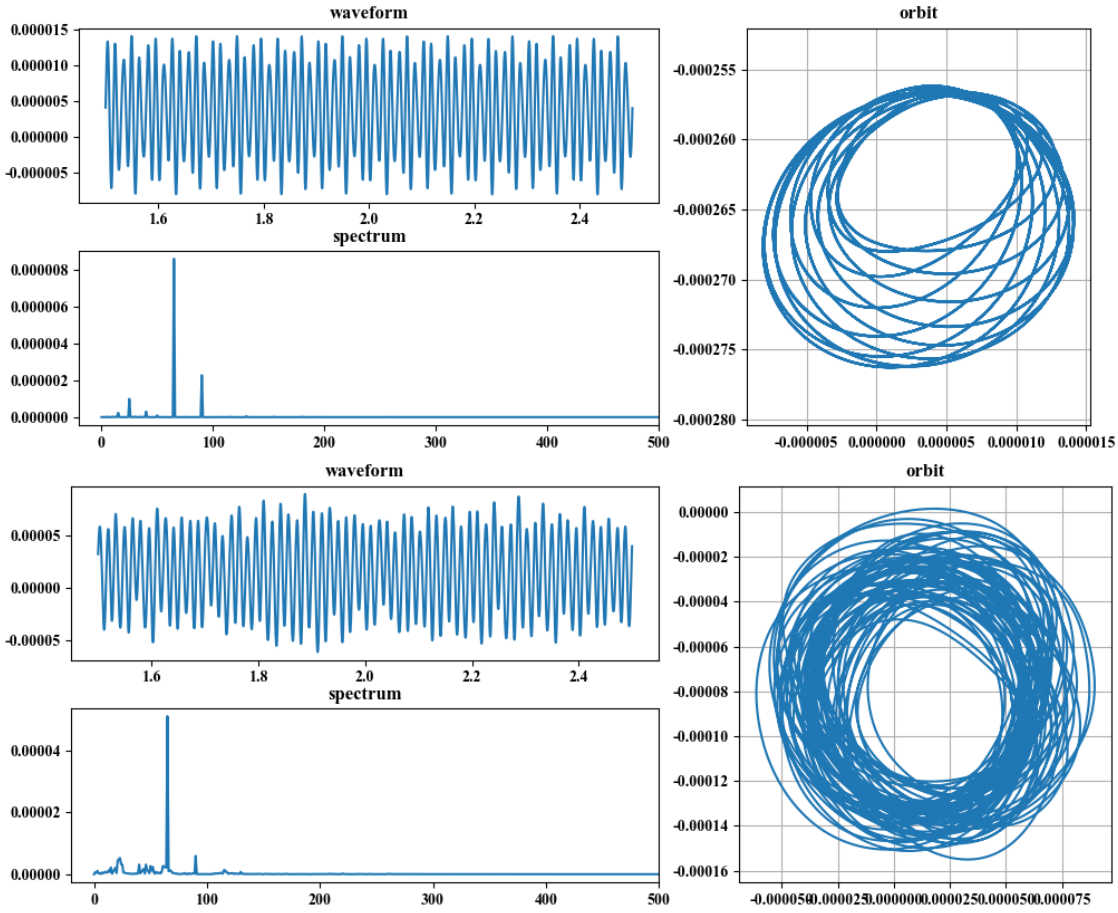

Figure 8. Waveform, spectrum and orbit of looseness fault, with or without SFD.

The displacement waveform, spectrum and shaft centerline orbit of node 15 on the inner rotor at the state of rub-impact fault is in Figure 9. When the clearance outside the inner rotor disc decrease, the disc will touch the bottom first because of the gravity effect, thus forms a state of single point rub-impact. Contact impacts make the shape of the shaft centerline orbit no longer close to a circle, and the amplitude of the inner rotor rotation frequency becomes more prominent. There are some frequency components in both low and high frequency areas due to the fault.

When there is no squeeze film damper, those low and high frequency components become more abundant. The shaft centerline orbit becomes less smooth. Like the situation of

looseness, SFDs weaken the impacts caused by the rub-impact fault.

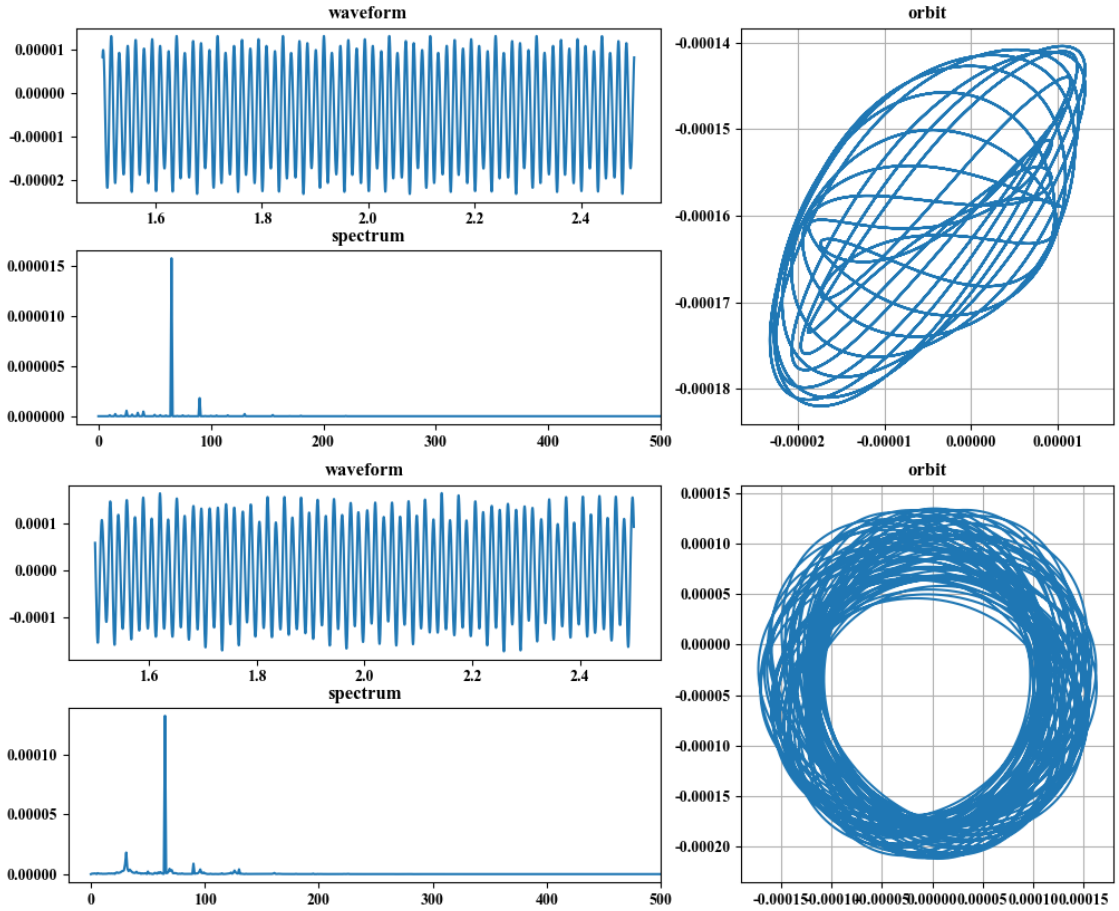

Figure 9. Waveform, spectrum and orbit of rub-impact fault, with or without SFD.

Figure 10 shows the situation when the unbalance fault and the looseness fault both exist, and the situation when the unbalance fault and the rub-impact fault both exist. The location and parameter of the faults are the same as single faults. The increase in the amount of unbalance increases the overall vibration amplitude of the rotor, thus enhances the nonlinear phenomena of the looseness or rub-impact fault. The fractional frequency components in the looseness fault and the low-frequency and high-frequency components in the rub-impact fault all become more significant.

Figure 11 shows the situation when the looseness fault and the rub-impact fault both exist, and the location and parameter of the faults are the same as single faults. The half rotational frequency component is much higher than single fault state of looseness or rub-impact. It can be said that in the presence of looseness, the constraint of the rotor is weakened and the rub-impact fault will cause more pronounced nonlinear phenomenon.

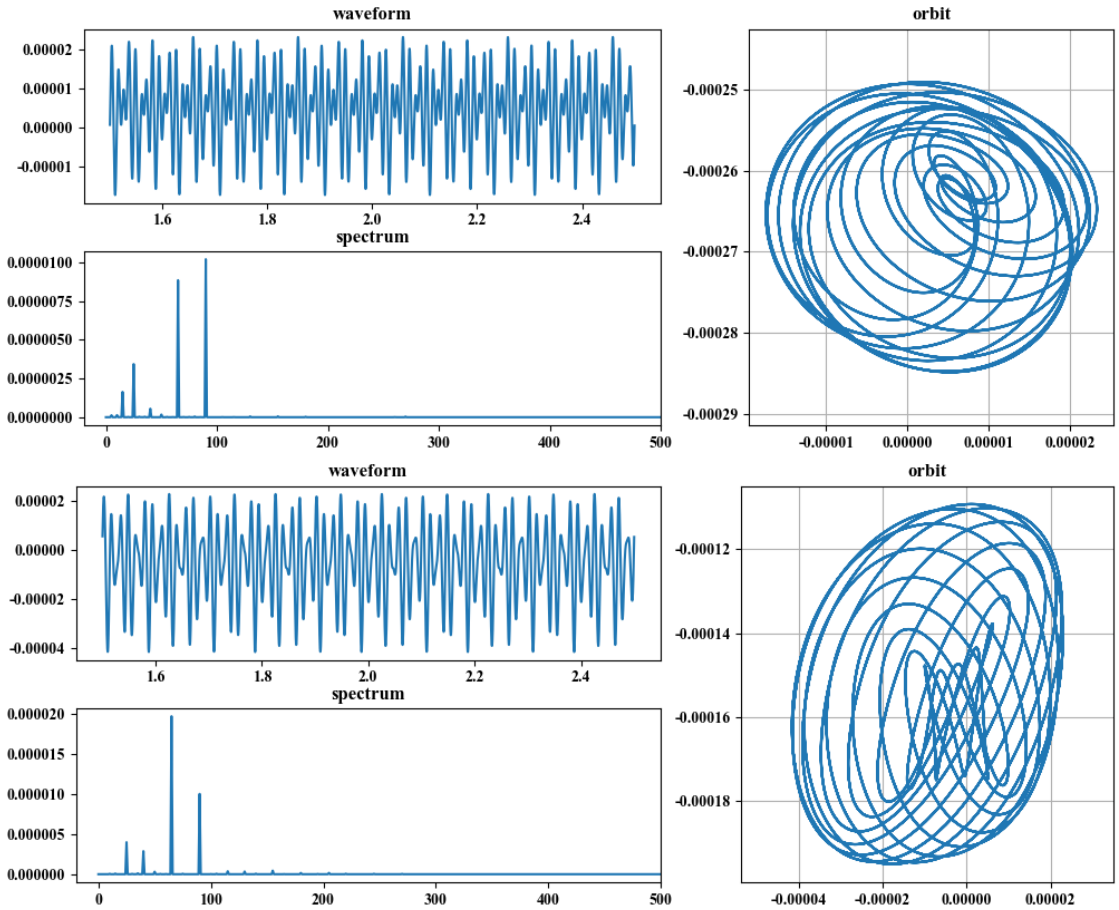

Figure 10. Waveform, spectrum and orbit of unbalance-looseness fault and unbalance-rub-impact fault.

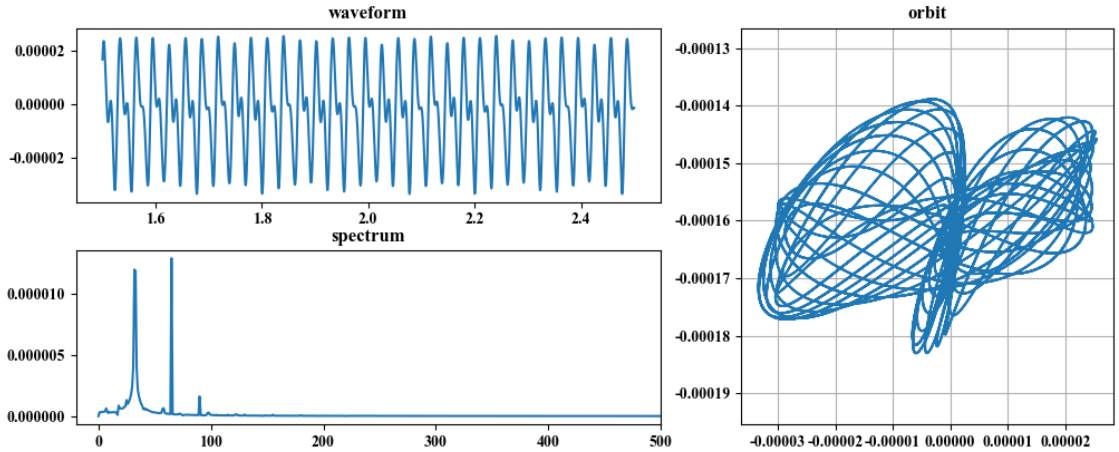

Figure 11. Waveform, spectrum and orbit of looseness-rub-impact fault.

Conclusion: This paper presents a finite element approximate model of an aero-engine dual-rotor system which includes nonlinear models of rolling element bearings and squeeze film dampers and can introduce single or multiple typical rotor faults in. The rolling

element bearing is using a kind of nonlinear multi-body dynamic model, and the squeeze film damper is using the fluid-film forces model based on the cavitated short bearing theory. Steady-state vibration response of the dual-rotor system shows main frequency components of the two rotation speed.

The typical rotor faults simulated include rotor unbalance, rotor misalignment, support looseness, and dynamic-static rub-impact. Those faults are introduced to the system by adding nonlinear forces to the generalized external force vector, and fault features are obtained by solving the system equation. The unbalanced fault causes an increase in the amplitude of the rotational frequency. The misalignment fault causes an increase in the amplitude of twice the rotational frequency. The looseness fault brings in fractional frequency components. The rub-impact fault brings in many low and high frequency components. SFDs could weaken the impacts caused by looseness or rub-impact. And the looseness fault and the rub-impact fault could enhance the nonlinear phenomenon of each other when they both exist.

Many parameters could have influences on the characteristics of rotor faults, including the rotor parameters like mass, stiffness, damping and rotation speed, or the fault parameters like the location and the severity of faults. This paper does not discuss all these parameters in detail. But interesting result might be attained by studying fault characteristics in a nonlinear dual-rotor system.

References:

[1] Chiang, H. W. D., Hsu, C. N., Jeng, W., Tu, S. H., & Li, W. C. (2002, January). Turbomachinery dual rotor-bearing system analysis. In ASME Turbo Expo 2002: Power for Land, Sea, and Air (pp. 803-810). American Society of Mechanical Engineers.

[2] Hai, P. M., & Bonello, P. (2008). An impulsive receptance technique for the time domain computation of the vibration of a whole aero-engine model with nonlinear bearings. Journal of Sound Vibration, 318(3), 592-605.

[3] Sinou, J. J. (2009). Non-linear dynamics and contacts of an unbalanced flexible rotor supported on ball bearings. Mechanism & Machine Theory, 44(9), 1713-1732.

[4] Chen, G. (2015). Vibration modelling and verifications for whole aero-engine. Journal of Sound & Vibration, 349, 163-176.

[5] Liu, M., & Gorman, D. G. (1995). Formulation of rayleigh damping and its extensions. Computers & Structures, 57(57), 277-285.

[6] Gupta, P. K. (1975). Transient ball motion and skid in ball bearings. Journal of Tribology, 97(2), 261.

[7] Sawalhi, N., & Randall, R. B. (2008). Simulating gear and bearing interactions in the presence of faults: part i. the combined gear bearing dynamic model and the simulation of localised bearing faults. Mechanical Systems & Signal Processing, 22(8), 1924-1951.

[8] Mohan, S., & Hahn, E. J. (1974). Design of squeeze film damper supports for rigid

rotors. Journal of Engineering for Industry, 96(3), 976.
[9] Burrow, C. R., Sahinkaya, M. N., Kucuk, N. C., & Taylor, D. (1987). Dynamic performance of squeeze-film bearings.
[10] Inayat-Hussain, J. I., Kanki, H., & Mureithi, N. W. (2003). On the bifurcations of a rigid rotor response in squeeze-film dampers. Journal of Fluids & Structures, 17(3), 433-459.
[11] Dewell, D. L., & Mitchell, L. D. (1984). Detection of a misaligned disk coupling using spectrum analysis. Journal of Vibration & Acoustics, 106(1), 9.
[12] Ma, H. (2011). Analysis of dynamic characteristics for a rotor system with pedestal looseness. Shock & Vibration, 18(1-2), 13-27.
[13] Muszynska, A., & Goldman, P. (1995). Chaotic responses of unbalanced rotor/bearing/stator systems with looseness or rubs. Chaos Solitons & Fractals, 5(9), 1683-1704.